APPLIED AND ENVIRONMENTAL MICROBIOLOGY, Aug. 1999, p. 3502–3511 Vol. 65, No. 8
0099-2240/99/$04.00+0

Depth Penetration and Detection of pH Gradients in Biofilms by Two-Photon Excitation Microscopy

JURRIEN M. VROOM,[1] KEES J. DE GRAUW,[1] HANS C. GERRITSEN,[1] DAVID J. BRADSHAW,[2]* PHILIP D. MARSH,[2,3] G. KEITH WATSON,[4] JOHN J. BIRMINGHAM,[4] AND CLIVE ALLISON[4]

University of Utrecht, Utrecht, The Netherlands,[1] and Centre for Applied Microbiology and Research, Salisbury SP4 0JG,[2] Leeds Dental Institute, Leeds LS2 9LU,[3] and Unilever Research, Port Sunlight Laboratory, Bebington, Wirral L63 3JW,[4] United Kingdom

Received 9 December 1998/Accepted 15 May 1999

Deep microbial biofilms are a major problem in many industrial, environmental, and medical settings. Novel approaches are needed to understand the structure and metabolism of these biofilms. Two-photon excitation microscopy (TPE) and conventional confocal laser scanning microscopy (CLSM) were compared quantitatively for the ability to visualize bacteria within deep in vitro biofilms. pH gradients within these biofilms were determined by fluorescence lifetime imaging, together with TPE. A constant-depth film fermentor (CDFF) was inoculated for 8 h at 50 ml · h^{-1} with a defined mixed culture of 10 species of bacteria grown in continuous culture. Biofilms of fixed depths were developed in the CDFF for 10 or 11 days. The microbial compositions of the biofilms were determined by using viable counts on selective and nonselective agar media; diverse mixed-culture biofilms developed, including aerobic, facultative, and anaerobic species. TPE was able to record images four times deeper than CLSM. Importantly, in contrast to CLSM images, TPE images recorded deep within the biofilm showed no loss of contrast. The pH within the biofilms was measured directly by means of fluorescence lifetime imaging; the fluorescence decay of carboxyfluorescein was correlated with biofilm pH and was used to construct a calibration curve. pH gradients were detectable, in both the lateral and axial directions, in steady-state biofilms. When biofilms were overlaid with 14 mM sucrose for 1 h, distinct pH gradients developed. Microcolonies with pH values of below pH 3.0 were visible, in some cases adjacent to areas with a much higher pH (>5.0). TPE allowed resolution of images at significantly greater depths (as deep as 140 μm) than were possible with CLSM. Fluorescence lifetime imaging allowed the in situ, real-time imaging of pH and the detection of sharp gradients of pH within microbial biofilms.

Biofilms form on a wide range of inert and living surfaces and are associated with a number of significant beneficial (e.g., wastewater treatment) and damaging (e.g., fouling, corrosion, and dental disease) processes (3). Consequently, there is considerable interest in developing methods to study the architecture of, and metabolism within, such biofilms. Imaging of biofilms began with van Leeuwenhoek's observations of dental plaque in the 17th century. The development of scanning electron microscopy (SEM) in the last 30 years has allowed imaging of the detailed structures of a wide range of biofilms; generally, such studies showed biofilms to have an apparently densely packed structure (see, for example, reference 32). The preparation of samples for SEM studies, however, involves extensive dehydration of the samples, whereas natural biofilms usually exist in a fully hydrated state. More recent studies have used other microscopic techniques, in particular, confocal laser scanning microscopy (CLSM), which allows the study of biofilms without drying procedures. Such studies have shown biofilms to have a more open architecture (9, 23), in which palisades of biofilm biomass were shown to be interspersed with water channels of lower density. CLSM has more recently been used to examine biofilms of dental plaque bacteria developed in vitro (7, 11). However, the penetration depth of CLSM into these samples was limited to around 20 to 40 μm, depending upon the density of the samples analyzed.

The limited depth penetration of CLSM can be overcome by employing two-photon excitation microscopy (TPE) (13), in which the fluorescent molecule is excited by the simultaneous absorption of two (near-) infrared photons. Due to the use of the longer-wavelength excitation light in TPE, a much higher penetration into the sample is obtained than in CLSM (6, 12). This, together with the reduced photobleaching of the fluorescent probes, makes TPE well suited for in-depth imaging studies of strongly scattering samples such as biofilms.

An important feature of biofilms is the development of gradients of key biochemical parameters. Thus, the microenvironment within a biofilm can differ markedly from the planktonic phase (10), and this heterogeneity may facilitate the coexistence of species with distinct physiological requirements. The biofilm nature of dental plaque allows the development of gradients of key biochemical parameters. Thus, anaerobic bacteria can flourish in biofilms, in overtly aerobic environments such as seawater (14), and in the oral cavity (26). Likewise, conditions of localized low pH (<5.5) must occur in dental plaque following sugar consumption for demineralization (and ultimately caries) to take place, while the pH of saliva overlying plaque remains near neutral.

Key gradients of ion concentrations can be visualized by means of fluorescence imaging. Ion-sensitive intensity probes may be used, where the fluorescence intensity of the probe is affected by the ion concentration. This approach, however, is less suitable for quantitative imaging, since the results can be compromised by compartmentalization or concentration of the probe. For this reason, ratio-based methods have been developed, utilizing the shift in the excitation or absorption spectrum upon binding of ions to the fluorescent probe (17, 37). At the beginning of this decade, fluorescence lifetime imaging was

* Corresponding author. Mailing address: Research Division, CAMR, Salisbury SP4 0JG, United Kingdom. Phone: (44) 1980 612732. Fax: (44) 1980 612731. E-mail: david.bradshaw@camr.org.uk.

TABLE 1. Compositions of mixed-culture biofilms

Species	Mean $\log_{10}$ CFU/disk ± SD (% of total) in biofilms at day:	
	10	11
Streptococcus mutans	6.11 ± 0.22 (1.0)	7.05 ± 0.19 (13.3)
Streptococcus oralis	6.78 ± 0.31 (4.9)	6.56 ± 0.08 (4.3)
Streptococcus sanguis	7.08 ± 0.09 (9.8)	6.83 ± 0.14 (8.0)
Lactobacillus rhamnosus	7.53 ± 0.17 (27.6)	6.20 ± 0.09 (1.9)
Actinomyces naeslundii	5.86 ± 1.24 (0.6)	5.78 ± 0.68 (0.7)
Porphyromonas gingivalis	2.33 ± 1.87 (0.0002)	2.48 ± 2.1 (0.0004)
Prevotella nigrescens	4.34 ± 2.28 (0.02)	1.5 ± 0.7 (0.00004)
Fusobacterium nucleatum	7.32 ± 0.64 (17.0)	7.63 ± 0.35 (50.4)
Neisseria subflava	4.97 ± 1.00 (0.08)	3.80 ± 0.13 (0.007)
Veillonella dispar	7.68 ± 0.16 (39.0)	7.26 ± 0.12 (21.5)
Total	8.11 ± 0.27	7.95 ± 0.16

introduced as an alternative contrast form in microscopy. In this method, the differences in fluorescence decay times are exploited to produce contrast in fluorescence images (5, 16, 27, 36). Fluorescence lifetime imaging yields results that are independent of the probe concentration, and several groups have demonstrated that it is well suited for the quantification of ion concentrations (29, 36).

This paper describes studies to assess the potential of TPE for the imaging of deep biofilms developed in vitro. In particular, we have studied quantitatively the improvement in penetration with TPE, compared to CLSM, and the feasibility of quantifying pH gradients in biofilms by using fluorescence lifetime imaging. Finally, the pH response of biofilm following sucrose overlay was monitored. A mixed-culture biofilm of 10 oral bacteria was used as a defined model system for this study (20).

MATERIALS AND METHODS

Bacterial strains and biofilm development. A mixed culture of 10 oral bacteria (Table 1) was grown in a chemostat system, as described previously (4). This chemostat was used to inoculate a constant-depth film fermentor (CDFF) (8) for 24 h at 50 ml · h^{-1}, in a way similar to that described by Kinniment et al. (20); the CDFF biofilms were developed on a modified glass coverslip contained within a machined polytetrafluoroethylene (PTFE) assembly (Fig. 1). Fresh mucin-based growth medium (BMM) (4) was supplied to the biofilms in the CDFF for 10 or 11 days, and the biofilms were then removed. The CDFF apparatus was sparged continuously with 5% CO_2 in nitrogen (approximately 200 ml · min^{-1}). The coverslip-PTFE assembly was transferred into a plastic universal containing damp tissue paper to prevent drying of the biofilms. The biofilms were transported to the University of Utrecht, Utrecht, The Netherlands; the glass coverslips were removed from the PTFE assembly; and the biofilms were examined microscopically from below by TPE or CLSM within 24 h of removal from the CDFF. All of the depths quoted in this paper are with respect to the coverslip glass surface (i.e., at the base of the biofilm). Thus, a depth of 5 μm in a 100-μm biofilm would be 95 μm from the biofilm-air interface. For microbiological evaluation, the biofilms were detached by scraping, and their microbial compositions were determined by using selective and nonselective agar media as described previously (4). Such counts were carried out with fresh biofilms and with biofilms stored in the same way for 24 h to determine their viability after this time.

Microscopes. (i) Two-photon microscope. In TPE (13) the fluorescent molecule is excited by the simultaneous absorption of two photons providing the energy to reach the excited state. TPE uses (near-) infrared photons to excite molecules with absorption bands in the UV or blue region of the spectrum. The (near-) infrared excitation light is much less scattered by the sample than blue or UV excitation light. Therefore, TPE offers great advantages over the use of conventional confocal microscopy for in-depth imaging of the highly scattering samples such as oral biofilms. The two-photon excitation probability is, in general, very small and has a quadratic dependence on the excitation intensity. This limits the excitation of fluorescent molecules to the focal point of the microscope objective, thus providing intrinsic three-dimensional resolution. Importantly, in TPE, photodamage processes such as photobleaching are also restricted to the focal point. In contrast, in CLSM imaging, photodamage occurs over the whole

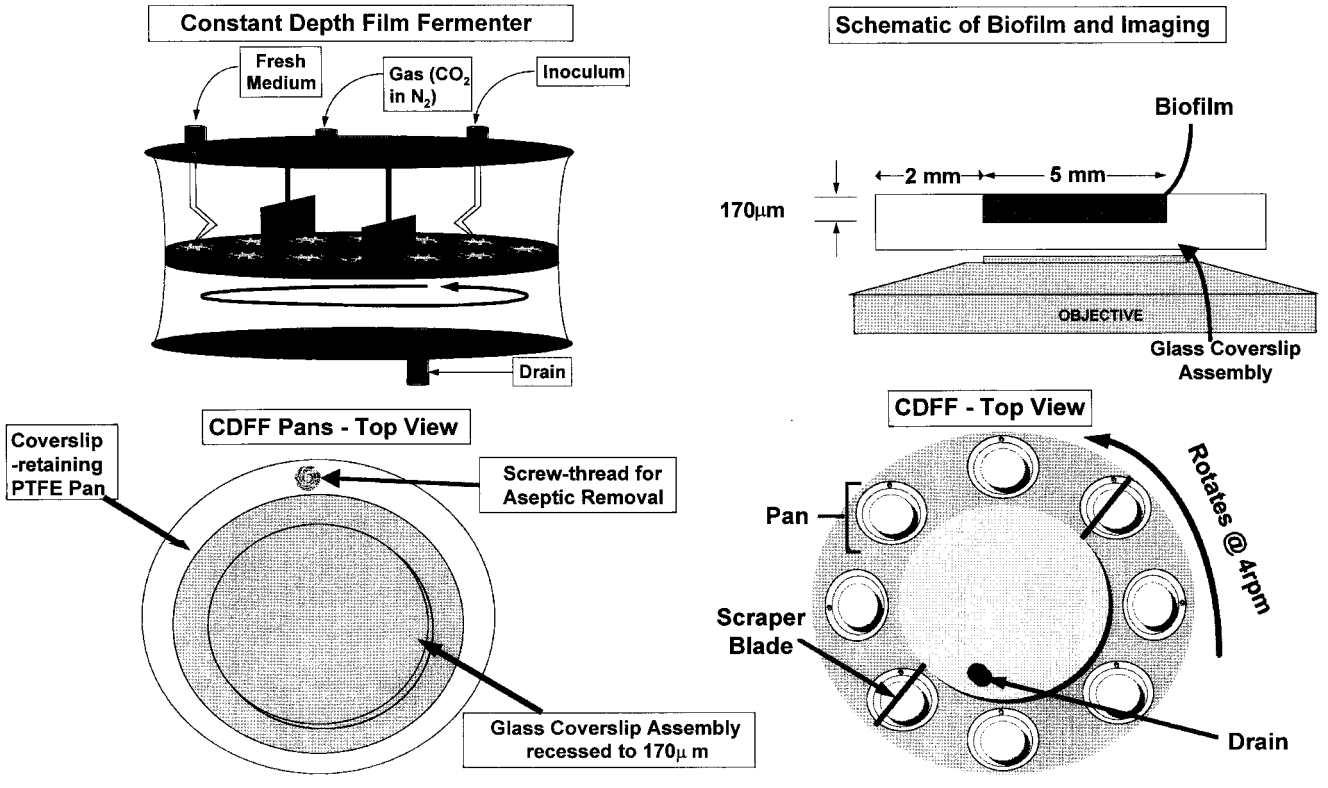

FIG. 1. CDFF apparatus, modified glass coverslip assembly, and imaging.

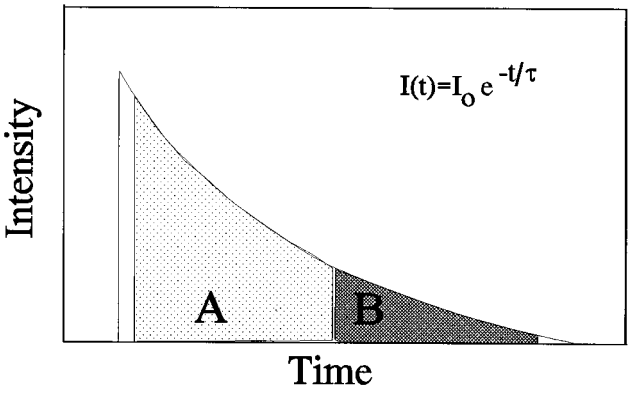

FIG. 2. Time-gated fluorescence lifetime imaging, in which the sample is excited with a brief excitation pulse, after which the fluorescence intensity is recorded in two (or more) time gates.

illumination cone. As a consequence, the recording of large three-dimensional images in a CLSM is seriously hampered. Due to the very small two-photon absorption cross-section, very high excitation intensities are required in order to produce sufficient fluorescence signal. To provide these high intensities, pulsed excitation (100 fs to 1 ps) is used in TPE, such that a high peak power is combined with a low time-averaged power. In this way, significant heating of the sample is avoided.

The TPE microscope used in this work was described in detail by Systma et al. (35). Briefly, the microscope is equipped with a titanium-sapphire laser pumped by a solid-state laser (both from Spectra Physics, Mountain View, Calif.). This light source produces an 0.6-W, 82-MHz pulse train of 80-fs pulses. The wavelength of the laser system is tunable between 700 and 1,000 nm such that a broad range of fluorescent probes can be excited. A fixed excitation wavelength of 800 nm was used for all of the TPE experiments described here. The homemade confocal microscope that we have used is based on an inverted geometry with the pinholes removed. Furthermore, a special dichroic mirror which reflects the infrared light of the laser (>700 nm) and transmits the fluorescent light (<700 nm) is used. Remaining excitation light in the detection path is removed by a series of 700-nm interference short-pass filters (Optosigma, Santa Ana, Calif.). In the quantitative pH imaging experiments, an additional band-pass filter (Omega Optical, Dallas, Tex.) that transmits fluorescence from 500 to 530 nm was added to reduce the autofluorescence background from the biofilm.

(ii) Fluorescence lifetime imaging. The detection system of the microscope is equipped with a fast photomultiplier tube (R1894; Hamamatsu K.K., Hamamatsu, Japan) and fast detection electronics capable of fluorescence lifetime determination. The method to determine the fluorescence lifetime is based on time-gated detection of the fluorescence and is schematically depicted in Fig. 2 for a simple monoexponential decay. After excitation of the fluorochromes with the laser pulse, the fluorescence is detected in two time windows (gates), one close to the excitation pulse and one delayed. The ratio of these intensities, I_A/I_B, is a measure of the fluorescence decay time. In the case of a monoexponential decay, the decay is described by $I_t = I_0 e^{-t/\tau}$ where I_0 and I_t are the fluorescence intensities at time 0 and time t, respectively, and τ is the fluorescence lifetime. For gates of equal width and separated in time by Δt, $\tau = \Delta t / ln(I_A/I_B)$. In the case of a multiexponential decay, this equation yields an average fluorescence lifetime value. A biexponential decay is often found in the case of ion-sensitive fluorescent dyes, where the dye usually exists in two forms, the free dye and ion-bound dye, each with its own lifetime. In this case, both lifetimes contribute to the fluorescence decay, with a weighting factor depending on the ion concentration. Therefore, the average lifetime is a unique measure of the ion concentration. In fluorescence lifetime imaging of ion concentrations, the instrument response, in terms of the ratio of the two window contents, I_A/I_B, is calibrated against the ion concentration.

(iii) Confocal microscope. Conventional confocal (single-photon excitation) fluorescence images were recorded with a commercial confocal scan head (PCM 2000; Nikon Corporation, Tokyo, Japan) mounted on an upright microscope body (Optiphot; Nikon Corporation). This confocal microscope is fiber connected to the light source, an Ar ion laser operating at 488 nm. The morphology experiments reported here were carried out with a 20-μm detection pinhole and a band-pass filter (Omega Optical) with a central wavelength of 590 nm and a width of 60 nm in the detection path.

All of the TPE imaging and calibration experiments as well as the CLSM experiments were carried out at room temperature, with the same plan-apochromatic water immersion objective with a numerical aperture of 1.2 (Nikon Corporation). A water immersion objective was used in order to minimize aberration caused by a mismatch in index of refraction between the biofilm specimen and the microscope objective.

Penetration depth, morphology, and resolution. To study the morphology of the biofilms, they were labelled with 50 μg of rhodamine B (Molecular Probes, Eugene, Oreg.) · ml^{-1} in water, followed by careful rinsing to remove free label. The biofilms were examined either with the TPE microscope, with an excitation wavelength of 800 nm, or with the conventional (single-photon excitation) confocal microscope. *xz* images (i.e., perpendicular to the surface of the specimen) of 100 by 95 μm at different lateral locations were recorded for the same samples. In addition, a number of *xy* images (i.e., parallel to the surface of the specimen) of 30 by 30 μm at different depths in the biofilm were recorded.

pH experiments. (i) Fluorescent probe and labelling. Only a limited number of fluorescent pH indicators are available for the quantitative imaging of pH in the acidic range. The probes that are suitable are all excitation ratio probes. These probes exhibit a characteristic shift in the excitation spectrum upon binding to H^+. Two measurements are carried out at different excitation wavelengths while the intensity is monitored at a fixed emission wavelength. The ratio of these two measurements is a quantitative measure of the H^+ concentration. TPE at two different wavelengths requires two separate laser systems and is therefore technically difficult and expensive. Moreover, at present it is not clear whether the TPE spectra of the current probes are compatible with excitation ratio imaging. We therefore opted for a quantitative imaging method based on fluorescence lifetimes.

Fluorescein was used for the quantitative (lifetime) imaging of pH. This molecule is completely ionized in aqueous solutions at above pH 9. Acidification progressively protonates fluorescein to different forms with specific spectral and lifetime characteristics. The pH range over which fluorescein can be used as a lifetime probe (15) is in the neutral-acidic range that is expected within the biofilm. Another advantage of fluorescein is the comparatively large cross-section for two-photon absorption at 800 nm (38). We used carboxyfluorescein because the charged carboxyl group prevents penetration of the probe through the bacterial membranes but does not alter the spectral properties of fluorescein (18). In this way, a contribution to the fluorescence signal corresponding with intracellular pH values is avoided.

(ii) pH calibration. The buffer solutions (pH 3, 4, 5, 6, and 7) for the calibration were prepared by mixing 0.1 M citric acid and 0.2 M Na_2HPO_4 solutions in different ratios to obtain the desired pH. The pH 8 buffer solution was prepared with a 0.1 M Tris buffer. NaCl was added to all buffer solutions to a final concentration of 100 mM. Carboxyfluorescein was purchased from Molecular Probes.

In order to study the influence of the local chemical environment in the biofilm on the pH calibration, calibrations were carried out in pH buffer and in biofilm immersed in an excess of buffer solution to set the pH. Comparison of these calibrations showed that the probe response was slightly affected by the biofilm environment (data not shown). Therefore, the calibration procedure to convert window ratios to pH values was performed in biofilm. For the pH calibration in biofilm, approximately 20 μl of biofilm was immersed in 0.5 ml of buffer solution of the desired pH containing carboxyfluorescein. Calibration images were recorded after 30 min of equilibration. Next, the average window ratio of the image was calculated. A calibration curve relating the average window ratio (I_A/I_B) of carboxyfluorescein to the pHs of buffers saturating the biofilm was constructed.

(iii) Autofluorescence. Preliminary experiments detected significant autofluorescence emitted by the biofilm. This can seriously hamper the quantification of pH. In order to minimize the autofluorescence contribution of the biofilm to the total fluorescence signal, the probe concentration in the biofilm should be as high as possible. Care has to be taken, however, since at a high probe concentration the fluorescence lifetime can be either lowered by self-quenching or raised by reabsorption of the emitted light (22). The influence of the probe concentration on the fluorescence lifetime was measured in buffer (pH 7) with probe concentrations of between 20 and 500 μM. The resulting lifetimes were found to be identical for all probe concentrations. Thus, to minimize the autofluorescence contribution while avoiding excessive probe concentrations due to probe binding within the biofilm, a probe concentration of 100 μM was chosen for the imaging experiments. Furthermore, an interference band-pass filter with a transmission band from 500 to 530 nm was inserted in the detection light path. This filter transmits 50% of the fluorescence of carboxyfluorescein and 20% of the autofluorescence. Another way to diminish the contribution of the autofluorescence, uniquely reserved to time gating, is to delay opening of the time gates. This possibility is based on the observation that the fluorescence decay times of autofluorescence are comparatively short, in general less than 1 ns. In our samples a delay of 1 ns between the excitation pulse and the opening of the first gate resulted in a reduction of the detected autofluorescence by 80%. The carboxyfluorescein signal, on the other hand, was reduced by only about 20%. Therefore, the 1-ns delay yields an improvement in signal-to-autofluorescence background of a factor of 4. The combination of the comparatively high probe concentration and the spectral and temporal suppression reduces the relative contribution of the autofluorescence to less than 2% of the total detected signal.

(iv) pH imaging experiments. In the pH experiments, the excitation intensity at the sample was controlled by a set of neutral density filters and varied between 5 mW (at the biofilm-coverslip interface) and 20 mW (at the 95-μm depth). For the fluorescence lifetime imaging, two time gates were used and their positions and widths were optimized empirically. The first gate started 1 ns after the laser pulse and had a width of 1 ns, while the second started 6 ns after the laser pulse

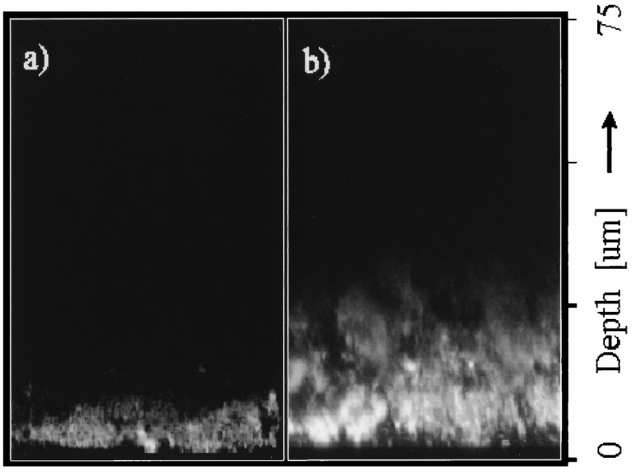

FIG. 3. Fluorescence penetration depth in *xz* sections of rhodamine B-stained biofilm by confocal (single-photon) imaging (a) and TPE (b). Depths are measured from the biofilm-coverslip interface.

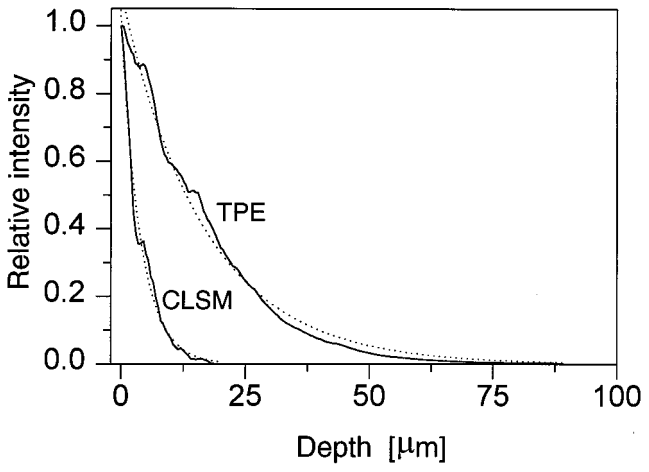

FIG. 4. Axial (*xz*) intensity profiles derived from Fig. 3.

and had a width of 5 ns. Frames of 256 by 256 pixels (16-bit resolution) were recorded, with pixel dwell times ranging from 512 μs to 2 ms.

Biofilms grown for 10 or 11 days were stained by adding an excess of the NaCl-carboxyfluorescein buffer solution to the biofilm specimen. The pH distribution of this untreated biofilm was thus determined. Identical biofilm samples were examined in this way, before and 1 h after the addition of the buffer-probe mixture supplemented with 14 mM sucrose. Sucrose was found not to affect the fluorescence lifetime of carboxyfluorescein. The possible effect of photobleaching on the lifetime of carboxyfluorescein in biofilm was also investigated. A line was continuously scanned over the sample for 5 min with twice the excitation intensity used for imaging. No changes in the lifetime were observed.

RESULTS

Microbiology. The microbial composition of typical 10- and 11-day-old biofilms, examined by TPE and CLSM, is shown in Table 1. In both sets of biofilms, complex communities of aerobic, facultative, and anaerobic bacteria developed. Other studies in our laboratory have confirmed that biofilm development in the CDFF system is reproducible between repeat runs when the chemostat inoculation system is used. Control studies also confirmed that viable counts of biofilm bacteria were unaffected after 24 h of storage (equivalent to the time required to transport the biofilms from the Centre for Applied Microbiology and Research, Salisbury, United Kingdom, to Utrecht) (data not shown).

Penetration depth, morphology, and resolution. The difference in penetration depth in rhodamine B-stained biofilm between confocal (single-photon) imaging and TPE imaging is illustrated in fluorescence *xz* images in Fig. 3. The images are normalized to the same maximum intensity. Figure 3a was recorded with the confocal (single-photon) microscope, and Fig. 3b was recorded with the two-photon microscope. These images clearly demonstrate the deeper penetration with TPE. The fluorescence intensity decay with depth was compared quantitatively by integrating these images in the *x* direction and scaling, yielding the axial intensity profiles displayed in Fig. 4. Both curves exhibit an approximately monoexponential decay, as demonstrated by the monoexponential fits. Overall, the penetration depth in these samples was increased by a factor of approximately four when TPE was employed. In practice, good-quality TPE images, in which individual bacterial cells were clearly distinguishable, could be recorded to depths of approximately 140 μm. A number of fluorescence *xy* images are shown in Fig. 5. Again the images are normalized to the same maximum intensity. Images were recorded from the same sample at different positions by CLSM and TPE at depths of 10, 40, and 60 μm. In both the confocal and the two-photon images, different shapes of bacteria can be observed, including long fusiform bacteria and cocci. In the image recorded at the 10-μm depth, predominantly coccoid bacteria forming a compact microcolony are visible. In the confocal images, both the contrast and the signal-to-noise ratio decrease as a function of depth, leading to a rapid loss of information for the deeper layers in the sample. In the TPE images, the contrast is conserved over the whole depth range. Only the signal-to-noise ratio decreases for the deeper layers in the biofilm.

For in-depth imaging, it is of the utmost importance that the index of refraction of the immersion liquid of the objective matches the index of refraction of the sample. A mismatch leads to spherical aberration, which progressively increases with depth. For this reason, we employed a water immersion objective. Experiments with an oil immersion objective yielded disappointing results. The resolution of the images rapidly degraded with depth, and in addition, the fluorescence intensity decayed more rapidly than that with the water immersion objective.

pH imaging. (i) pH calibration of window ratios. The pH calibration curve is shown in Fig. 6. The window ratio was found to have a sigmoidal dependence on pH and increased with decreasing pH. The fact that window ratios near unity were found is a result of the unequal widths of the time gates: the first and second windows have widths of 1 and 5 ns, respectively. The calibration images (not shown) yielded pH values independent of depth, thus showing that the 30-min incubation time was sufficient for the biofilm to equilibrate with the pH buffer. Despite the absence of nutrients in the pH calibration buffer added to the biofilm, some heterogeneity in the calibration images was noted. The heterogeneity is apparent as regions coinciding with individual bacteria, or groups of bacteria, with a lower pH and a fluorescence intensity slightly higher than average. The standard deviation of the calibration is estimated to be less than 0.4 pH unit for pH 6 to 8, 0.5 pH unit for pH 5, and up to around 1 pH unit for pH 3. We note that as the pH goes down, the quantum efficiency of fluorescein goes down. At pH 3, a fluorescence intensity 20-fold-lower than that at pH 8 was observed. The fluorescence intensity relative to that at pH 8 is also given in Fig. 6.

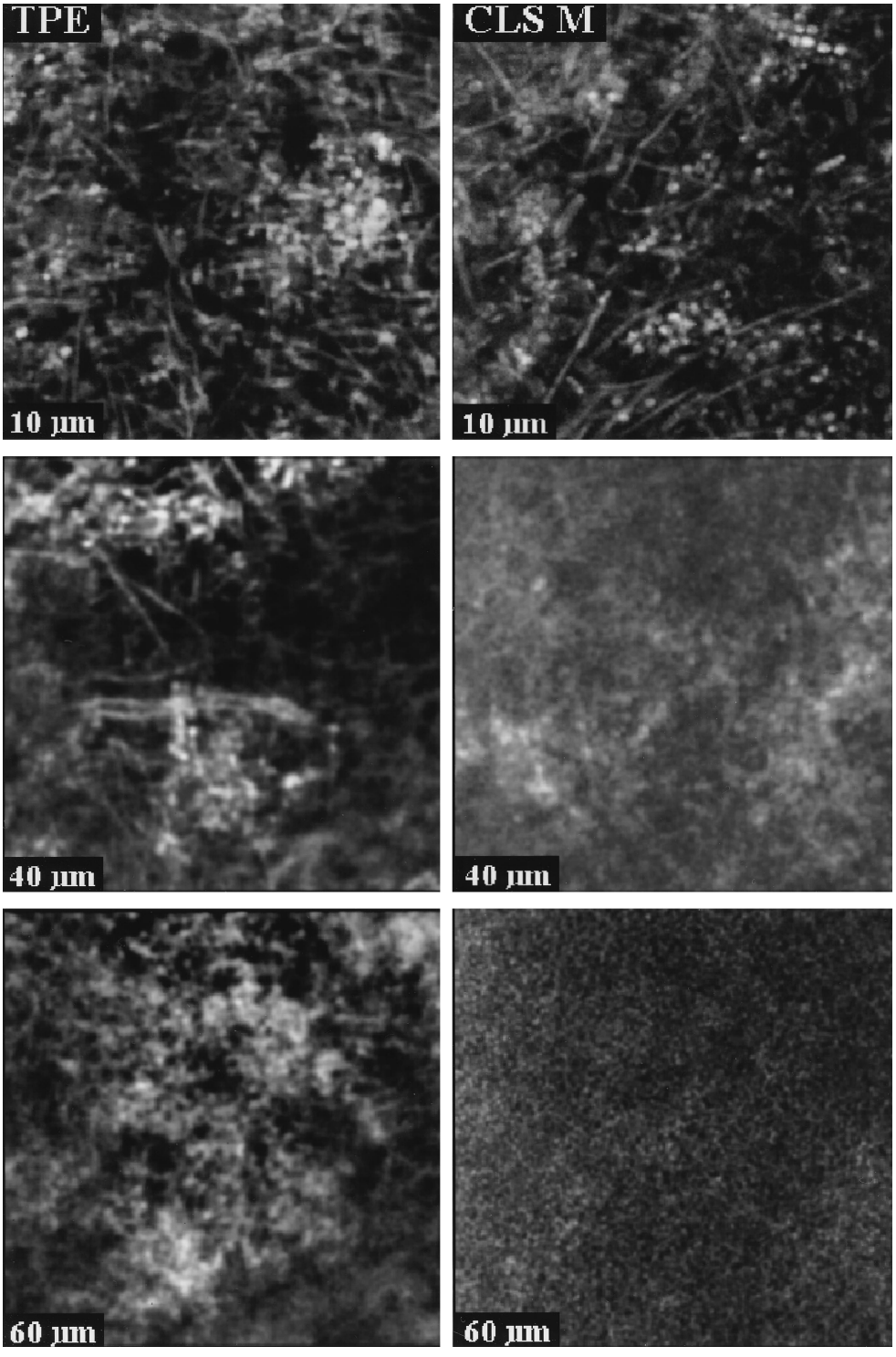

FIG. 5. Fluorescence *xy* images of 30 by 30 μm recorded at distances of 10, 40, and 60 μm from the biofilm-coverslip interface (see Fig. 1) by using CLSM (right) and TPE (left).

(ii) pH imaging in untreated biofilm. In Fig. 7A and C, *xy* images of areas of 30 by 30 μm at the 5- and 70-μm depths, respectively, are shown. These images were recorded by using the coverslip assembly shown schematically in Fig. 1. Note that depth is defined with respect to the coverslip-biofilm interface. The thickness of this biofilm was approximately 100 μm. A depth of 5 μm in the biofilm thus corresponds to 95 μm from the biofilm-buffer interface. The bacteria are visible in the fluorescence intensity image, indicating a heterogeneous distribution of carboxyfluorescein. In some places the fluorescence intensity in the vicinity of the bacteria is two to three times the average intensity of the rest of the image, suggesting

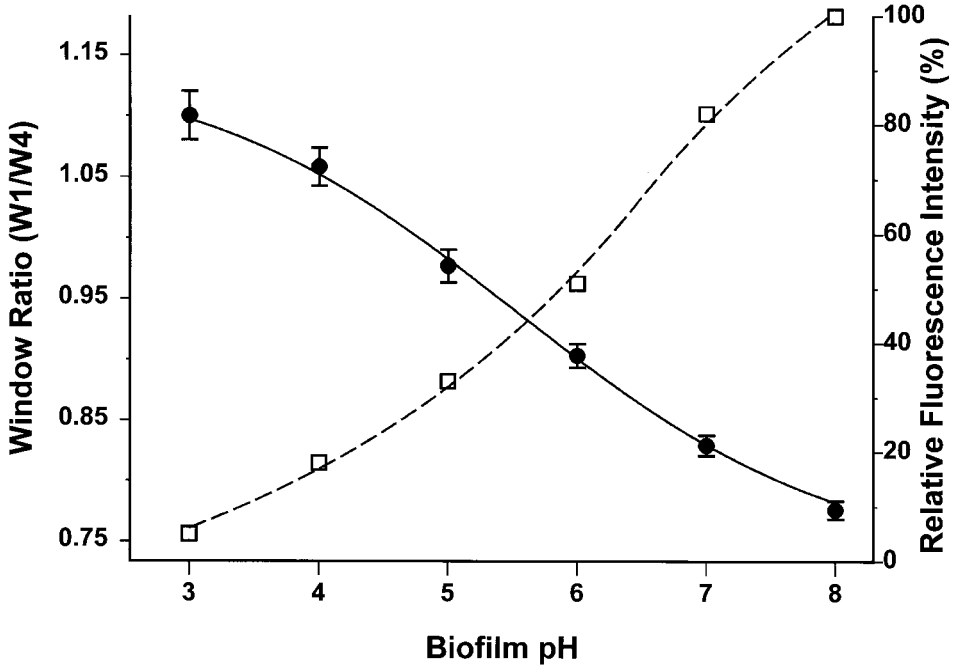

FIG. 6. Solid line, relation between biofilm pH and window ratio (W_1/W_4), with data points fitted to a Boltzmann sigmoidal curve: $y = [(A_1 A_2)/(1 + e^{(x - x_{50})/dx})] + A_2$, where A_1 and A_2 are the asymptotes, x_{50} is the center, and dx is the width ($\chi^2 = 3 \times 10^{-5}$). The error bars reflect the variability (standard deviation) of three independent calibration experiments. Dashed line, relative fluorescence intensity of carboxyfluorescein as a function of pH.

that probe molecules may have become concentrated on the bacterial surfaces.

The pH (window ratio) image at the 5-μm depth shows a homogeneous pH over the 30- by 30-μm area, with an average pH of 7.0 ± 0.3 (Fig. 7B). The pH image at the 70-μm depth (image not shown) yielded an average pH of 6.0 ± 0.4.

To visualize the axial gradient, a 50- by 95-μm *xz* image was recorded, and to improve the image statistics for the deeper layers, the original image of 256 by 256 pixels was 4-by-4 binned, to yield a 64- by 64-pixel image. In the resulting image, a clear axial gradient can be observed (Fig. 8). At the biofilm-buffer interface (the top of the image), an average pH of 5.9 ± 0.4 was found, while the average pH in the deeper layers (i.e., closer to the biofilm-coverslip interface) was 7.2 ± 0.4.

(iii) pH imaging following sucrose overlay. Following sucrose overlay, the bacteria in the biofilm generated acids by fermentation, thus lowering the pH. Figure 9 shows *xy* intensity and pH images before and 1 h after sucrose application. The images are 70 by 70 μm and were recorded at the 35-μm depth. Figure 9A and C show the intensity and pH images, respectively, prior to application of a 14 mM sucrose solution; Fig. 9B and D show the corresponding intensity and pH images, respectively, recorded 1 h later. The average pH fell from 6.2 initially to 5.5 1 h after the addition of sucrose. Some of the coccoid bacteria in Fig. 9B were associated with particularly high fluorescence intensities (approximately 10 to 20 times the average). At the same positions in the window ratio (pH) image in Fig. 9D, pH values that fall outside the calibration range (pH of <3.0) were found. Addition of excess buffer of pH 3 to the biofilm resulted in disappearance of the bright spots.

In Fig. 10 the average pH over areas comprising 100 by 100 pixels at three different depths are shown as a function of time. Since the pH at the bright spots cannot be quantified reliably,

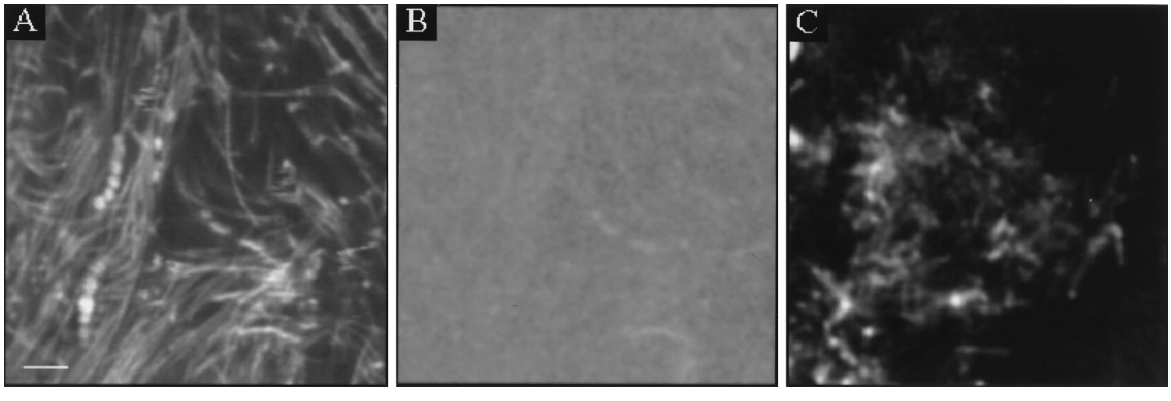

FIG. 7. TPE *xy* images of biofilms at 5 μm (A) and 70 μm (C) from the biofilm-coverslip interface. (B) pH image of panel A. Bar, 5 μm.

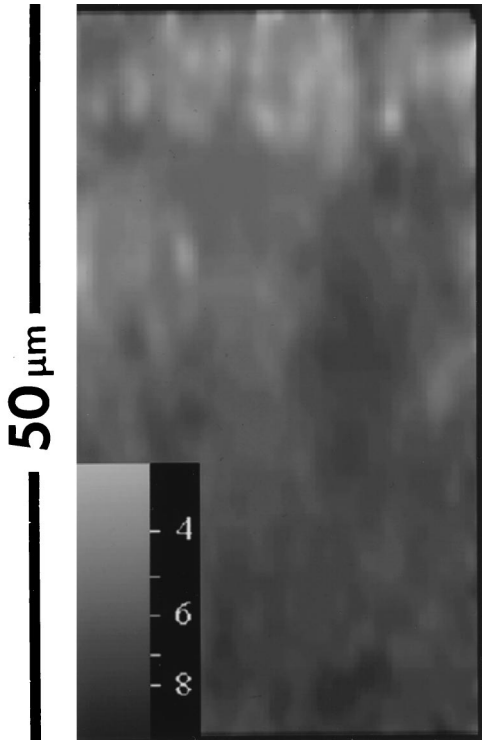

FIG. 8. Window ratio (pH) image of an *xz* section through biofilm. A higher intensity (lighter image) in the window ratio images indicates a lower pH value. The top of the image is the biofilm-buffer interface; the bottom represents the biofilm-coverslip interface.

the corresponding pixels in the window ratio image were excluded from the pH-averaging calculation. However, a clear decrease of the pH was observed as a function of time. In addition, the layers at depths of 35 and 70 μm (i.e., closer to the biofilm–buffer-sucrose interface) showed a significantly lower pH than those at 5 μm (near the coverslip).

DISCUSSION

TPE versus CLSM. In this study we have compared the utilities of CLSM and TPE for the imaging of thick microbial biofilms produced in a CDFF apparatus. From the comparison of fluorescence intensity decays as a function of imaging depth (Fig. 4), a fourfold improvement in penetration was found for this specific sample by using TPE. However, this compares only average fluorescence intensities, and the image quality is not taken into account. In the confocal images, we found a significant loss of contrast when imaging the deeper layers in the biofilm. This effect is well known for confocal imaging and is caused by scattering effects (31). In confocal imaging, fluorescence light emitted outside the focal volume is suppressed by the pinhole in front of the detector. Fluorescence light generated outside the focal volume may, however, be scattered in a direction that is imaged onto the detector pinhole. This out-of-focus background leads to a loss of contrast. The magnitude of the background depends on the amount of scattered light and is related to the properties of the sample and the imaging depth into the sample. The size of the bacteria with respect to the wavelength is particularly important; shorter wavelengths give rise to stronger scattering. In contrast, TPE generates all fluorescence at the focal spot, so scattering of fluorescence light does not degrade the image quality. Consequently, the factor of four for the improvement in penetration depth is a conservative estimate. In practice, we have been able to record TPE images of biofilm at 140 μm. At this depth, the fluorescence intensity was 15 times higher than that with the confocal microscope. Images at even greater depths can be recorded by increasing the integration time and/or laser power.

pH calibration. Conventional fluorescence methods for the quantification of pH are not compatible with TPE. Fluorescence lifetime imaging was combined, therefore, with TPE to carry out the quantitative in-depth pH imaging experiments. The accuracy of the calibration was reduced at lower pH. The reason for the limited accuracy is probably the local chemical environment of the probe. Binding, for instance, to specific proteins may somewhat alter the fluorescence behavior of the probe. Furthermore, we cannot entirely exclude the existence of small local pH gradients in the calibration images. However, this may not be very likely, since the excess buffer used to equilibrate the pH in the biofilm did not contain nutrients. Moreover, the magnitude of the heterogeneity observed was reproducible. Finally, the fluorescence intensity of carboxyfluorescein strongly depends on the pH (Fig. 6). Knowledge about this effect is helpful for estimating probe concentrations.

pH gradient imaging. pH gradients in the biofilm were quantified in both the axial and lateral directions. Clear pH gradients were observed in the *z* direction (Fig. 7 and 8), and the magnitude of these gradients was well above the accuracy of the calibration. No such pH gradients were visible in the calibration images. The axial pH gradient visible in the *xz* image (Fig. 8) is assumed to be due to bacterial metabolic activity. The NaCl-carboxyfluorescein buffer that was used for staining the biofilm is slightly acidic and has a mild pH-buffering capacity. This forces the pH in the biofilm near the buffer to be slightly acidic. The axial gradients were more pronounced than those in the lateral direction. This was expected, since the limitations on diffusion of nutrients and of key metabolites such as oxygen and solutes, etc., are likely to be more uniform in the *xy* plane than in the *xz* direction (26). It was also notable that in Fig. 8 several bands of approximately constant pH were observed. This can again be attributed to differences in diffusion between the *xy* and *xz* planes in the biofilm.

In TPE images of biofilms, spatial heterogeneity was observed in the fluorescence intensity; individual bacteria were distinguished separately (Fig. 7A and C). This could be the result of changes in the quantum efficiency of the carboxyfluorescein but also of accumulation and concentration of probe on bacterial surfaces. However, the pH image was homogeneous within 0.4 pH unit (Fig. 7B), indicating that the quantum efficiency of carboxyfluorescein was constant. Therefore, we conclude that probe molecules must have accumulated on the bacterial surfaces, leading to the comparatively high fluorescence intensities at these locations. Previous studies have described the use of fluorescence intensity-based probes to measure oxygen or pH in biofilms (reviewed in references 9 and 10). Here, carboxyfluorescein also was used as a pH probe. These intensity-based methods rely on uniform distribution of the probe throughout the biofilm matrix and are not suitable for quantitative measurements. We have demonstrated that probe may become concentrated on the surface of bacterial cells in our in vitro biofilms. In addition, although more recent studies of biofilms have suggested a relatively open structure (23), with water channels interspersed among bacterial microcolonies (10), the microcolonies within biofilms are known to restrict the diffusion of many molecules. The accuracy of intensity-based methods is thus limited by the very heterogeneity and diffusion limitation properties which are of such fundamental interest in studying biofilms. In contrast, since the flu-

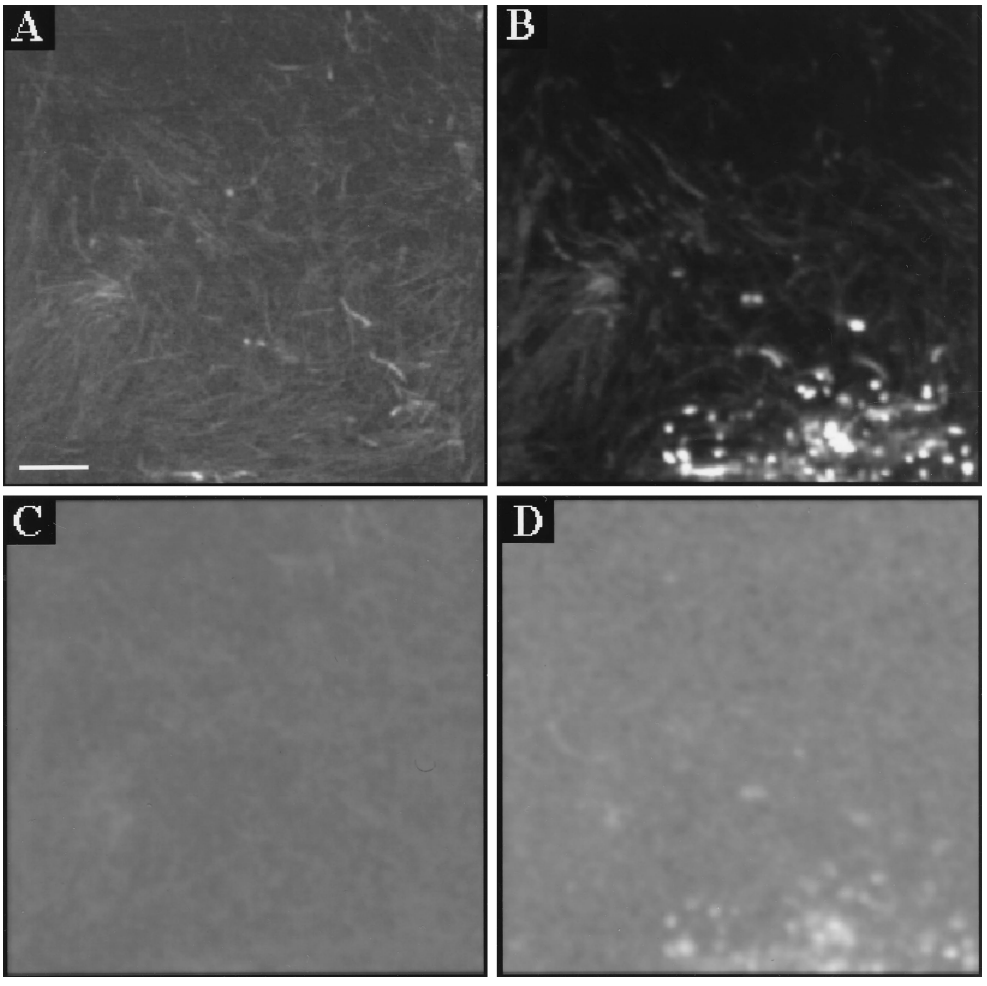

FIG. 9. Intensity (A and B) and window ratio (pH) (C and D) images in biofilm, before (A and C) and 60 min after (B and D) addition of a 14 mM sucrose solution. Images were recorded at 65 μm from the surface. The average pH values are 6.2 for panel C and 5.5 for panel D. Bar, 10 μm.

orescence lifetime method described here is independent of probe concentration, this technique offers a significant advantage in determining key ion concentrations in heterogeneous biofilms.

pH gradients following sucrose overlay. After the overlay of sucrose, the pH in the biofilm was reduced over time. One hour after the addition of sucrose, brightly fluorescing microcolonies were observed in the fluorescence intensity image. The observed fluorescence intensity was 10- to 20-fold higher than the average intensity in the image. At the same positions in the window ratio (pH) image, pH values that fall outside the calibration range are found (pH of <3.0). This is well below the average pH (ca. 5.5) in the pH image. This observation is surprising, since such a high fluorescence intensity is not expected at low pH. At pH 3.0, the quantum efficiency of carboxyfluorescein is about six times lower than that at pH 5.5. Consequently, a carboxyfluorescein concentration of between 6 and 12 mM (i.e., 10 to $20 \times 6 \times 100$ μM) at the position of the bright spots is implied. At such high probe concentrations, fluorescence quenching may occur, leading to a reduction of the observed fluorescence lifetime and a lowering of the apparent pH. When excess buffer of pH 3 was added to the biofilm, the bright spots disappeared. This suggests that the local pH at these bright spots was below pH 3. The mechanisms by which diffusion of organic acids (lactate would be likely to be the predominant acid end product of sucrose catabolism) may be restricted in these biofilms are not yet known. Previous studies of molecular transport phenomena in oral biofilms have indicated relatively little hindrance of diffusion in thinner biofilm structures (ca. 20 μm) (33).

The observations at very low pH can be explained by local precipitation of the carboxyfluorescein at a pH of less than 3. This could be caused by full protonation of the dye in the most acidic regions of the biofilm. At these exceptionally bright spots the pH cannot be reliably quantified; therefore, the corresponding pixels in the window ratio images were excluded in the analysis of the time-dependent pH measurements (Fig. 10). As expected, the pH fell with time at all depths following sucrose fermentation. The lowest pH value found, pH 5.5, is therefore biased conservatively due to the exclusion of the hot spots.

Alternative (direct) methods for pH determination. The alternative to fluorescence-probe based methods for pH or ion determinations is methods based on either in-dwelling or micro-touch electrodes, especially for pH measurement. A number of practical and theoretical problems can arise with their use. Microelectrodes are not that small in relation to the scale of the bacterial biofilms that they are intended to study. Generally, 0.1-mm (i.e., 100-μm) tips have been used in studying dental plaque biofilms (30), although oxygen microelectrodes

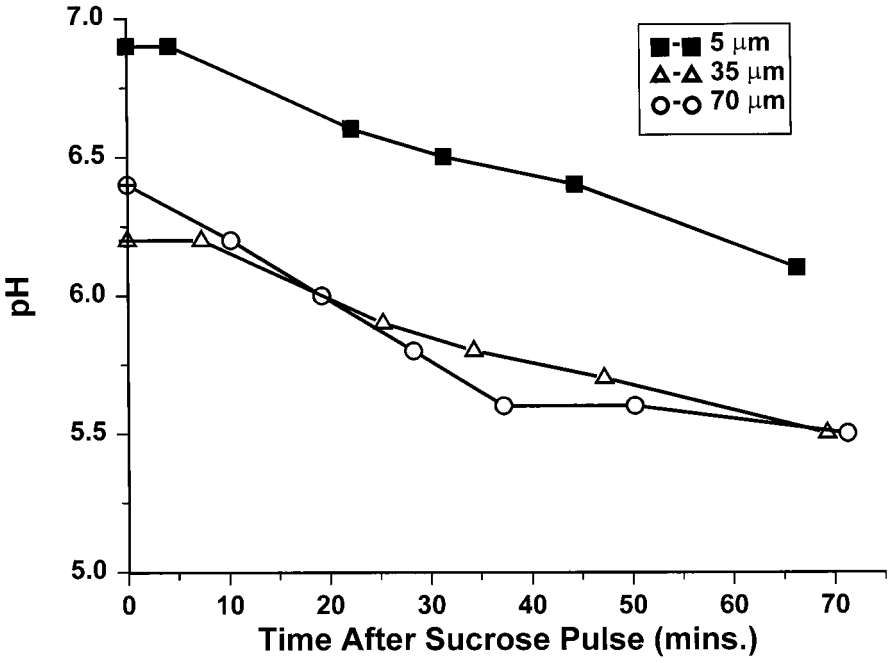

FIG. 10. Decrease in mean biofilm pH in a 100-μm biofilm following a sucrose pulse. The average pH over 30-by 30-μm *xy* images (100 by 100 pixels) at 70, 35, and 5 μm from the biofilm-coverslip assembly is shown.

with tips of <10 μm have been described (28). Often, far larger microelectrodes are used. The accurate insertion and positioning of the probes into the biofilm to be measured pose considerable practical problems, and the structure of the biofilm itself may be compromised by the insertion of the electrode. In addition, although electrodes are often assumed to provide an absolute measure of pH, a systematic study of a widely used microelectrode revealed highly variable accuracy and precision between different electrodes (21).

In-dwelling electrodes have been used to measure the pH at the base of biofilms developing on teeth. Such electrodes are often larger than microelectrodes (34), and the assumption that biofilm develops on the electrode in a manner similar to that on the surrounding tooth surface is made. In the case of in-dwelling (telemetric) electrodes, although studies indicate a correlation between pH values determined following plaque sampling and from in-dwelling electrodes (19), this approach has been questioned more recently (1). In-dwelling electrodes appear to give greater pH responses than micro-touch electrodes, but there may be serious problems related to calibration of these electrodes. In addition, in-dwelling electrodes cannot measure pH changes at locations within the overlying biofilm structure.

Implications for future biofilm studies. A novel technique for optical imaging of pH in oral biofilms has been described. The images presented in this paper demonstrate the development of distinct gradients of pH within mixed-culture oral biofilms. These gradients were detectable even when the biofilms had only BMM as a growth substrate (i.e., in the absence of readily fermentable carbohydrate sources). Here, the pH of the biofilm at the carboxyfluorescein-NaCl buffer interface is fixed by the mildly acidic properties of this buffer. When sucrose was overlaid on the biofilms for 1 h, the pH fell sharply. This pH fall was associated with the development of distinct gradients; at some locations, the pH fell to surprisingly low levels. While previous imaging studies using SEM have indicated a complex heterogeneous population structure (2, 20), the relationship between this structure and local metabolic effects has not been described previously.

The demonstration of zones of distinct heterogeneity in pH through the biofilm (in both the *xy* and *xz* planes) may provide a mechanism to explain the coexistence of the range of species with dramatically different requirements for growth found in biofilms such as dental plaque. The difficulties in demonstrating bacterial specificity associated with dental decay have often been assumed to be related to the inherent complexity and variability of the oral microflora (25). The findings in this study imply that zones of low pH might allow mutans streptococci to flourish locally, while the overall plaque pH was relatively neutral and the pH-lowering potential of plaque was limited. Conversely, the detection of pH-sensitive bacteria in carious lesions (i.e., sites with a low pH) may also be explained by compartmentalization of zones of different pH within the dental plaque biofilm. Such heterogeneity could also explain the existence of microorganisms in apparently hostile conditions (e.g., sulfate-reducing bacteria in aquatic environments) (14, 24).

Conclusions. TPE is a powerful tool for in-depth imaging of biofilms. The depth range over which images can be recorded is at least four times greater than that with conventional confocal microscopy. The practical usefulness of images from TPE is enhanced even further because of improved contrast at deeper layers compared to CLSM.

TPE is not compatible with conventional fluorescence methods to quantify pH. However, pH can be quantified by means of fluorescence lifetime imaging with carboxyfluorescein. This technique allows determination of pH (and potentially of concentrations of other ions of interest) independently of the probe concentration. The need for such an approach in the study of biofilms has been discussed previously (9). The pH images demonstrated that microzonal variations of pH exist in our mixed-culture biofilms. These pH gradients were more

pronounced in untreated biofilms in the axial (*xz*) than in the lateral (*xy*) direction. After the addition of sucrose, sharper pH gradients were detectable, and very-low-pH microcolonies became visible. The pH of the colonies was below the lowest value of the usable range of fluorescein as a pH probe.

The techniques described here still require practical and theoretical refinements. However, the work presented here has provided key insights into the complexity of structural and microbiological factors affecting pH changes in biofilms. This approach could be applied to a range of biofilms associated with a variety of industrial and environmental habitats.

REFERENCES

1. **Baelum, V., O. Fejerskov, and A. Küseler.** 1994. Approximal plaque pH following topical applications of standard buffers *in vivo*. Caries Res. **28:**116–122.
2. **Barber, P., A. Boyd, H. N. Newman, S. J. Challacombe, T. P. Vrahopoulos, and S. Gill.** 1990. Immunogold labelling of *Porphyromonas gingivalis* in pure culture and in apical border plaque. Microb. Ecol. Health Dis. **3:**217–222.
3. **Brading, M., J. Jass, and H. M. Lappin-Scott.** 1995. Dynamics of bacterial biofilm formation, p. 46–63. *In* H. M. Lappin-Scott and J. W. Costerton (ed.), Plant and microbial biotechnology research series, no. 5. Microbial biofilms. Cambridge University Press, Cambridge, United Kingdom.
4. **Bradshaw, D. J., A. S. McKee, and P. D. Marsh.** 1989. Effects of carbohydrate pulses and pH on population shifts within oral microbial communities *in vitro*. J. Dent. Res. **68:**1298–1302.
5. **Buurman, E. P., R. Sanders, A. Draaijer, H. C. Gerritsen, J. J. F. van Veen, P. M. Houpt, and Y. K. Levine.** 1992. Fluorescence lifetime imaging using a confocal laser scanning microscope. Scanning **14:**152–159.
6. **Centonze, V. E., and J. White.** 1998. Multiphoton excitation provides optical sectioning from deeper within scattering specimen than confocal imaging. Biophys. J. **75:**2015–2024.
7. **Cook, G. S., J. W. Costerton, and R. J. Lamont.** 1998. Biofilm formation by *Porphyromonas gingivalis* and *Streptococcus gordonii*. J. Periodontal Res. **33:** 323–327.
8. **Coombe, R. A., A. Tatevossian, and J. W. T. Wimpenny.** 1981. Bacterial thin films as *in vitro* models for dental plaque, p. 239–249. *In* R. M. Frank and S. A. Leach (ed.), Surface and colloid phenomena in the oral cavity. IRL Press, London, United Kingdom.
9. **Costerton, J. W., Z. Lewandowski, D. E. Caldwell, D. R. Korber, and H. M. Lappin-Scott.** 1995. Microbial biofilms. Annu. Rev. Microbiol. **49:**711–745.
10. **Costerton, J. W., Z. Lewandowski, D. DeBeer, D. E. Caldwell, D. R. Korber, and G. James.** 1994. Biofilms, the customized microniche. J. Bacteriol. **176:** 2137–2142.
11. **Cummins, D., M. C. Moss, C. L. Jones, C. V. Howard, and P. G. Cummins.** 1992. Confocal microscopy of dental plaque development. Binary **4:**86–91.
12. **Denk, W., D. W. Piston, and W. W. Webb.** 1995. Two-photon molecular excitation in laser scanning microscopy, p. 445–458. *In* J. Pawley (ed.), Handbook of biological confocal microscopy, 2nd ed. Plenum, New York, N.Y.
13. **Denk, W., J. Strickler, and W. W. Webb.** 1990. Two-photon laser scanning fluorescence microscopy. Science **248:**73–76.
14. **Dexter, S. C.** 1993. Role of microfouling organisms in marine corrosion. Biofouling **7:**97–127.
15. **French, T., P. T. C. So, D. J. Weaver, T. Coehlo-Sampaio, E. Gratton, E. W. Voss, and J. Carrero.** 1997. Two-photon fluorescence lifetime imaging microscopy of macrophage-mediated antigen processing. J. Microsc. **185:**339–353.
16. **Gadella, T. W. J., T. M. Jovin, and R. M. Clegg.** 1993. Fluorescence lifetime imaging microscopy (FLIM)—spatial resolutions of microstructures on the nanosecond time scale. Biophys. Chem. **48:**221–239.
17. **Grynkiewicz, G., M. Poenie, and R. Y. Tsien.** 1985. A new generation of Ca^{2+} indicators with greatly improved fluorescence properties. J. Biol. Chem. **260:**3340–3450.
18. **Haugland, R. P.** 1996. Handbook of fluorescent probes and research chemicals, 6th ed. Molecular Probes, Eugene, Oreg.
19. **Jensen, M. E., P. J. Polansky, and C. F. Schachtele.** 1982. Plaque sampling and telemetry for monitoring acid production on human buccal tooth surfaces. Arch. Oral Biol. **27:**21–31.
20. **Kinniment, S. L., J. W. T. Wimpenny, D. Adams, and P. D. Marsh.** 1996. Development of a steady-state microbial biofilm community using the constant depth film fermenter. Microbiology **142:**631–638.
21. **Küseler, A., V. Baelum, O. Fejerskov, and J. Heidmann.** 1993. Accuracy and precision *in vitro* of Beetrode microelectrodes used for intraoral pH measurements. Caries Res. **27:**183–190.
22. **Lakowicz, J. R.** 1986. Principles of fluorescence microscopy. Plenum Press, New York, N.Y.
23. **Lawrence, J. R., D. R. Korber, B. D. Hoyle, J. W. Costerton, and D. E. Caldwell.** 1991. Optical sectioning of microbial biofilms. J. Bacteriol. **173:** 6558–6567.
24. **Lee, W., Z. Lewandowski, P. H. Nielsen, and W. A. Hamilton.** 1995. Role of sulfate-reducing bacteria in corrosion of mild steel: a review. Biofouling **8:**165–194.
25. **Loesche, W. J.** 1986. Role of *Streptococcus mutans* in human dental decay. Microbiol. Rev. **50:**353–380.
26. **Marsh, P. D., and D. J. Bradshaw.** 1995. Dental plaque as a biofilm. J. Ind. Microbiol. **15:**169–175.
27. **Morgan, C. G., A. C. Mitchell, and J. G. Murray.** 1990. Nano-second time-resolved fluorescence microscopy: principles and practice. Trans. R. Microsc. Soc. **90:**463–466.
28. **Revsbech, N. P., and D. M. Ward.** 1983. Oxygen microelectrode that is insensitive to medium chemical composition: use in an acid microbial mat dominated by *Cyanidium caldarium*. Appl. Environ. Microbiol. **45:**755–759.
29. **Sanders, R., A. Draaijer, H. C. Gerritsen, P. M. Houpt, and Y. K. Levine.** 1995. Quantitative pH imaging in cells using confocal fluorescence lifetime imaging microscopy. Anal. Biochem. **227:**302–308.
30. **Scheie, A. A., O. Fejerskov, P. Lingstrom, D. Birkhed, and F. Manji.** 1992. Use of palladium touch microelectrodes under field conditions for *in vivo* assessment of dental plaque pH in children. Caries Res. **26:**44–51.
31. **Schmitt, J. M., M. L. E. Knüttel, and M. Yadlowsky.** 1994. Confocal microscopy in turbid media. J. Opt. Soc. Am. A **11:**2226–2235.
32. **Silverstone, L. M., N. W. Johnson, J. M. Hardie, and R. A. D. Williams.** 1981. The formation, structure and microbial composition of dental plaque, p. 70–102. *In* L. M. Silverstone, N. W. Johnson, J. M. Hardie, and R. A. D. Williams (ed.), Dental caries: aetiology, pathology and prevention. Macmillan Press, London, United Kingdom.
33. **Singleton, S., R. Treloar, P. Warren, G. K. Watson, R. Hodgson, and C. Allison.** 1997. Methods for microscopic characterization of oral biofilms: analysis of colonization, microstructure and molecular transport phenomena. Adv. Dent. Res. **11:**133–149.
34. **Smit, A., M. Pollard, P. Cleaton-Jones, and A. Preston.** 1997. A comparison of three electrodes for the measurement of pH in small volumes. Caries Res. **31:**55–59.
35. **Systma, J., J. M. Vroom, H. Gerritsen, and Y. Levine.** 1995. The development of a confocal laser scanning microscopy using two-photon excitation in combination with time-gated detection. Soc. Photo. Instr. Eng. J. **2412:**110–114.
36. **Szmacinski, H., and J. R. Lakowicz.** 1993. Optical measurements of pH using fluorescent lifetimes and phase-modulation fluorometry. Anal. Chem. **65:** 1668–1674.
37. **Tsien, R. Y., and M. Poenie.** 1986. Fluorescence ratio imaging: a new window into intracellular ionic signaling. Trends Biochem. Sci. **11:**450–455.
38. **Xu, C., and W. W. Webb.** 1996. Measurement of 2-photon excitation cross sections of molecular fluorophores with data from 690 to 1050nm. J. Opt. Soc. Am. B **13:**481–491.